

Acceleration of Plasma Flows in the Solar Atmosphere Due to Magnetofluid Coupling - Simulation and Analysis

Swadesh M. Mahajan¹

Institute for Fusion Studies, The University of Texas at Austin, Austin, Texas 78712

Nana L. Shatashvili²

*Plasma Physics Department, Tbilisi State University, Tbilisi 380028, Georgia
International Center for Theoretical Physics, Trieste, Italy*

Solomon V. Mikeladze and Ketevan I. Sigua

Andronikashvili Institute of Physics, Georgian Academy of Sciences, Georgia

ABSTRACT

Within the framework of a two-fluid description possible pathways for the generation of fast flows (dynamical as well as steady) in the lower solar atmosphere is established. It is shown that a primary plasma flow (locally sub-Alfvénic) is accelerated when interacting with emerging/ambient arcade-like closed field structures. The acceleration implies a conversion of thermal and field energies to kinetic energy of the flow. The time-scale for creating reasonably fast flows ($\gtrsim 100$ km/s) is dictated by the initial ion skin depth while the amplification of the flow depends on local β . It is shown, for the first time, that distances over which the flows become "fast" are $\sim 0.01 R_s$ from the interaction surface; later the fast flow localizes (with dimensions $\lesssim 0.05 R_s$) in the upper central region of the original arcade. For fixed initial temperature the final speed ($\gtrsim 500$ km/s) of the accelerated flow, and the modification of the field structure are independent of the time-duration (life-time) of the initial flow. In the presence of dissipation, these flows are likely to play a fundamental role in the heating of the finely structured Solar atmosphere.

Subject headings: Sun: atmosphere — Sun: chromosphere — Sun: corona — Sun: magnetic fields — Sun: transition region — Acceleration of Particles

¹Electronic mail: mahajan@mail.utexas.edu

²Electronic mail: shatash@ictp.trieste.it nanas@iberiapac.ge

1. Introduction

In astrophysics (particularly in the physics of the solar atmosphere), plasma "flow" could be assigned at least two connotations: 1) The flow is a primary object whose dynamics bears critically on the phenomena under investigation. The problems of the formation and the original heating of the coronal structure, the creation of channels for particle escape, for instance, fall in this category, 2) The flow is a secondary feature of the system, possibly created as a by-product and/or used to drive or suppress an instability. Since the generation of flows which will eventually create the coronal structures (Mahajan *et al.* 1999; Mahajan *et al.* 2001) is the theme of this effort, the flows here are fundamental.

By exploiting a simple two-fluid model in the solar context, several recent studies (Mahajan & Yoshida 1998; Yoshida & Ohsaki & Mahajan 2004) have revealed the breadth of phenomena made possible by the combined action of the flow-velocity and the magnetic fields. The flow-based approach will prove, perhaps, crucial in the study of solar corona, observationally found to be a highly dynamic arena replete with multiple-scale spatiotemporal structures (Aschwanden *et al.* 2001a); the approach gains immense credibility with the discovery that strong flows are found everywhere – in the subcoronal (chromosphere) as well as in the coronal regions (see e.g. (Schrijver *et al.* 1999; Winebarger & DeLuca & Golub 2001; Aschwanden *et al.* 2001a; Aschwanden 2001b; Seaton *et al.* 2001; Winebarger *et al.* 2002; Feldman & Landi & Curdt 2003; Brynildsen *et al.* 2004) and references therein). Recent phenomenology strongly emphasizes that the solar atmosphere is an extremely inhomogeneous (in all parameters) area in which small- and large-scale closed magnetic field structures with different temperatures co-exist in nearby regions. For example, two-temperature coronal models constructed from *SOHO/EIT* observations indicate complicated magnetic topology and fine-scale structuring of corona (including Coronal Holes) (Zhang *et al.* 1999; Chertok *et al.* 2002). It is also clear that the mechanisms for energy transport and channeling of particles in Solar atmosphere are deeply connected with the challenging and exciting problems of the solar coronal heating and of the origin of the solar wind (SW) (Woo & Habbal & Feldman 2004).

If flows are to play an important and essential role in determining the dynamics and structure of the solar corona, we must immediately face the problem of finding sources and mechanisms for the creation of these flows. Catastrophic models of flow production in which the magnetic energy is suddenly converted into bulk kinetic energy (and thermal energy) are rather well-known; various forms of magnetic reconnection (flares, micro and nano-flares) schemes permeate the literature (E.g. (Wilhelm 2001; Christopoulou, Georgakilas and Koutchmy 2001) for chromosphere up-flow generations). A few other mechanisms of this genre also exist: Uchida *et al.* (2001) proposed that the major part of the supply of energy

and mass to the active regions of the corona may come from a dynamical leakage of magnetic twists produced in the sub-photospheric convection layer; Ohsaki *et al.* (2001, 2002) have shown how a slowly evolving closed structure (modelled as a double-Beltrami two-fluid equilibrium) may experience, under appropriate conditions, a sudden loss of equilibrium with the initial magnetic energy appearing as the mass flow energy. Another mechanism, based on loop interactions and fragmentations and explaining the formation of loop threads, was given in Sakai and Furusawa (2002); the suggestion based on cascade of shock wave interactions was made in (Ryutova & Tarbell 2003). A more quasi-static mechanism for flow generation in sub-coronal regions taking into account the density in-homogeneity of the structures was given in (Mahajan *et al.* 2002).

Before we embark on delineating the flow-generation mechanisms, we present additional evidence/speculation on their existence as well as their possible role in the processes taking place in the solar vicinity:

1) Goodman (2001) has shown that the mechanism which transports mechanical energy from the convection zone to the chromosphere (to sustain its heating rate) could also supply the energy needed to heat the corona, and accelerate the SW. The coronal heating problem, hence, is shifted to the problem of the dynamic energization of the chromosphere. In the latter process the role of flows is found to be critical as warranted by the following observations made in soft X-rays and extreme ultraviolet (EUV) wavelengths, and recent findings from the *Transition Region and Coronal Explorer (TRACE)*: the over-density of coronal loops, the chromospheric up-flows of heated plasma, and the localization of the heating function in the lower corona (Schrijver, *et al.* 1999; Aschwanden *et al.* 2001a; Aschwanden 2001b).

2) The connection/coupling of transient events like up-flows and different type jet-like structures to the photosphere dynamics was reported in numerous studies (see e.g. (Ryutova & Tarbell 2003) and references in). In (Liu *et al.* 2003) it was demonstrated that the eruptions of coronal mass ejection is triggered from the low solar atmosphere (photosphere/chromosphere) as seen in TRACE 1600Å images and with SOHO Michelson Doppler Imager. The data of this latest research favor the idea that a catastrophic loss of MHD equilibrium can be the primary driving mechanism for the rapid ejection that has 3 important stages - a relatively stable equilibrium, a loss (fast, impulsive) stage, and the final rapid eruption (associated with substantive changes in the photospheric magnetic flux and white-light morphology). The results of (Socas-Navarro & Martinez Pillet & Lites 2004) suggest the coupling between magnetic fields and convective processes that pervades the solar photosphere. The correlation between photospheric shear flows and flares is also reported in (Yang *et al.* 2004); several current models suggest that the former can be responsible for the energy build up of the flares.

3) In (Nitta & Cliver & Tylka 2003), the authors report on the low coronal signatures of major solar energetic particle (SEP) events focusing on flare-associated motions (observed in soft X-rays). It was underlined that these motions may provide an important link between small-scale energy release and large-scale explosive events; the existence of a continuum of acceleration timescales was pointed out. In (Magara & Longscope 2003) the detailed investigation of the dynamical behavior of emerging magnetic flux using three-dimensional MHD numerical simulation was carried out and it was shown that the emergence generates not only vertical but also horizontal flows in the photosphere, both of which contribute to the injection of the magnetic energy and helicity. The contributions of vertical flows are dominant at the early phase of flux emergence, while horizontal flows become a dominant contributor later. In (Falconer *et al.* 2003) it was shown that solar corona is mainly heated by the magnetic activity in the edges of the network flux clumps that are observed to be riddled with the fine-scale explosive events. They present that: (1) at the edges of the network flow clumps there are many transient sheared-core bipoles of the size and lifetime of granules and having transverse field strengths greater than $\sim 100 G$, (2) ~ 30 of these bipoles are present per supergranule, and (3) most spicules are produced by explosions of these bipoles.

4) Recent observations also suggest that the energy for coronal heating is very likely a by-product of the outflow of heat from Sun's interior through the convection zone – the convection zone acts as a heat engine, converting some of the thermal energy into mechanical and magnetic energy, some of which enters the corona and dissipates into heat. There are only two obvious energy sources that could power significant flow generation in the chromosphere: the magnetic field (both large scale and short-scale including turbulence), and the thermal pressure of the plasma. We have already mentioned a few examples of the magnetically driven transient, but sudden flow-generation. A more quiescent pathway was studied in (Mahajan *et al.* 2002) showing the possibility of magneto-fluid rearrangement of a relatively constant kinetic energy (going from an initial high-density-low-velocity state to a low-density-high-velocity stage). The mechanisms based on the wave-energy transformation and instabilities can be operative at later stages of the flow evolution; these mechanisms could have additional importance for acceleration (Poedts & Rogava & Mahajan 1998).

The main message then, is that to solve the coronal heating problem, the inclusion of processes taking place in the chromosphere and the transition region may be essential. In particular, one must take into account the different time-scale dynamical stages of the evolution of the primary flow as it passes through specific regions of solar atmosphere areas nested by varying scale ambient magnetic field structures. The dynamics of the flow must be understood.

In present paper we will show the possibility of flow acceleration/generation in the Solar atmosphere based on the dynamical two–fluid model suggested in (Mahajan *et al.* 2001). We will show that there exists an extremely fast stage (right at the lower chromosphere heights) giving rise to significant flow acceleration/generation; it is followed by a quasi–static stage in which the created fast flows are further accelerated via the magnetofluid coupling (depending on the region of the atmosphere the density could be constant or spatially varying). The detailed nature of accelerated flows will depend on the initial and boundary conditions.

2. Model

The physical model for flow generation/acceleration is a simplified two–fluid model. The plasma is quasi–neutral — electron and proton number densities are nearly equal: $n_e \simeq n_i = n$ ($\nabla \cdot \mathbf{j} = 0$), but the electron and the proton flow velocities are allowed to be different. Neglecting electron inertia, these are V_i and $V_e = (V - j/en)$, respectively. We assign equal temperatures to the electron and the protons so that the kinetic pressure p is given by: $p = p_i + p_e \simeq 2nT$, $T = T_i \simeq T_e$. The analysis can be readily extended later to the more realistic case of different temperatures for different species (McKenzie & Sukhorukova & Axword 1998). We understand that when solving the solar wind problem one should use the multi–fluid, multi–dimensional descriptions (see e.g. (Tu & Marsch 1997; Tu & Marsch 2001; Hollweg 1999) and references therein) but we however, believe, that essential features of the primary flow–based physics of its acceleration can be captured with our basic model. Very near the photospheric surface, the influence of neutrals and ionization (and processes of flux emergence etc.) would not permit just two–fluid approach. A little farther distance ($\Delta r \geq 500$ km) from the surface, however, we expect that there exist fully ionized and magnetized plasma structures such that the dynamical two–fluid model will capture the essential physics of flow generation.

The dimensionless two–fluid equations describing the flow–field interaction processes can be read from (Mahajan *et al.* 1999, 2001):

$$\frac{\partial}{\partial t} \mathbf{V} + (\mathbf{V} \cdot \nabla) \mathbf{V} = \frac{1}{n} \nabla \times \mathbf{b} \times \mathbf{b} - \beta_0 \frac{1}{n} \nabla (nT) + \nabla \left(\frac{rA_0}{r} \right) + \nu_i(n, T) \left(\nabla^2 \mathbf{V} + \frac{1}{3} \nabla (\nabla \cdot \mathbf{V}) \right), \quad (1)$$

$$\frac{\partial}{\partial t} \mathbf{b} - \nabla \times \left(\mathbf{V} - \frac{\alpha_0}{n} \nabla \times \mathbf{b} \right) \times \mathbf{b} = \alpha_0 \beta_0 \nabla \left(\frac{1}{n} \right) \times \nabla (nT), \quad (2)$$

$$\nabla \cdot \mathbf{b} = 0, \quad (3)$$

$$\frac{\partial}{\partial t} n + \nabla \cdot n \mathbf{V} = 0, \quad (4)$$

$$\begin{aligned} \frac{3}{2}n\frac{d}{dt}(2T) + \nabla(\mathbf{q}_i + \mathbf{q}_e) &= -2nT\nabla \cdot \mathbf{V} + 2\beta_0^{-1}\nu_i(n, T)n \left[\frac{1}{2} \left(\frac{\partial V_k}{\partial x_l} + \frac{\partial V_l}{\partial x_k} \right)^2 - \frac{2}{3}(\nabla \cdot \mathbf{V})^2 \right] \\ &+ \frac{5}{2}\alpha_0(\nabla \times \mathbf{b}) \cdot \nabla T - \frac{\alpha_0}{n}(\nabla \times \mathbf{b})\nabla(nT) + E_H - E_R. \end{aligned} \quad (5)$$

where the notation is standard with the following normalizations: the density n to n_0 at some appropriate distance from the solar surface, the magnetic field to the ambient field strength at the same distance, and velocities to the Alfvén velocity V_{A0} . The parameters $r_{A0} = GM_\odot/V_{A0}^2R_\odot = 2\beta_0/r_{c0}$, $\alpha_0 = \lambda_{i0}/R_\odot$, $\beta_0 = c_{s0}^2/V_{A0}^2$ are defined with n_0 , T_0 , B_0 . Here c_{s0} is a sound speed, R_\odot is the solar radius, $r_{c0} = GM_\odot/2c_{s0}^2R_\odot$, $\lambda_{i0} = c/\omega_{i0}$ is the collisionless skin depth, $\nu_i(n, T)$ is ion kinematic viscosity and q_e and q_i are electron and ion dimensionless heat flux densities, E_H is the local mechanical heating function and E_R is the total radiative loss. We note that the full viscosity tensor relevant to a magnetized plasma is rather cumbersome, and we do not display it here. Just to have a feel for the importance of spatial variation in viscous dissipation, we display its relatively simple symmetric form. It is to be clearly understood that this version is meant only for theoretical elucidation and not for detailed simulation. We also note that in general, Hall current contributions are expected to become significant when the dimensionless Hall coefficient α_0 satisfies the condition: $\alpha_0 > \eta$, where η is the inverse Lundquist number for the plasma. For a typical coronal plasma as well as for low chromosphere and transition region (TR) this condition is easily satisfied (α_0 is in the range $10^{-10} - 10^{-7}$ for densities within $(10^{14} - 10^8) \text{ cm}^{-3}$ and $\eta = c^2/(4\pi V_{A0}R_\odot\sigma) \sim 10^{-14}$, where σ is the plasma conductivity).

To establish the relevant parameter regime, we resort to recent observational data (e.g. (Goodman 2001; Aschwanden *et al.* 2001a; Socas-Navarro & Sanchez Almeida 2002) and references therein). At $\sim (500 - 5000) \text{ km}$, the observations yield the average plasma density and temperature to be respectively $n \sim (10^{14} - 10^{11}) \text{ cm}^{-3}$, and $T \sim (1 - 6) \text{ eV}$. For simplicity, we have assumed $T_e = T_i = T$. The information about the magnetic field is hard to extract due to the low sensitivity and lack of high spatial resolution of the measurements coupled with the inhomogeneity and co-existence of small- and large-scale structures with different temperatures, (observational evidence of small scale mixtures of weak and strong fields (Socas-Navarro & Lites 2004)) in nearby regions. The observation of pixel-to-pixel variations in the magnetic field indicates that small-scale (sub-pixel) distribution of fields changes considerably at larger spatial scales (Socas-Navarro & Sanchez Almeida 2003; Socas-Navarro 2004). At these distances we have different values for the network and for the internetwork fields: (i) The *network* plasmas have typically *short-scale* fields in the range $B_0 \sim (700 - 1500) \text{ G}$, have more or less $n \sim \text{const}$. (ii) The *internetwork fields* are generally weaker (with some exceptions (Socas-Navarro & Sanchez Almeida 2002)) — $B_o \leq 500 \text{ G}$,

and are embedded in *larger-scale plasma structures* with $n \neq \text{const}$. For different classes of magnetic field structures different scenarios may be operative.

3. Acceleration of particle flows – analysis of the stages

In our investigation we shall assume that the processes that generate the primary flows and the primary solar magnetic fields are independent. The plasma flows begin to interact with the ambient field at time $t=0$. The choice of initial conditions for our numerical work is guided by the observational evidence presented in the introduction. Our approach is consistent with that of Woo, Habbal and Feldman (2004) who have argued that the flow of the solar wind is influenced by the closed field structures stressing the self-consistent process of acceleration and trapping/heating of plasma particles in the finely structured atmosphere. We will dwell, in this paper, on the representative problem of the trapping and acceleration of the primary flow impinging on a single closed-line structure. The simulation was performed for a variety of initial and boundary conditions and essential aspects of the typical results will be presented below.

3.1. Dynamical generation of fast flows

The general set of Eqs. (1–5) was solved numerically in Cartesian Geometry for 2.5 Dimensions ($\partial_y = 0$). Note that the 2.5D Cartesian nature of our code does not allow us to explore large distances from the surface due to interference with the boundaries. Fortunately that does not translate into a serious shortcoming because much of the action is found to be limited to regions very close to the surface; the simulation results, therefore, are quite trustworthy in the revelation of the basic processes of interest. In carrying out the simulations an important assumption was made: the diffusion time of magnetic field is longer than the duration of the interaction process.

A short summary of our numerical methods is in order. We use the 2.5D version of Lax–Wendroff finite difference numerical scheme along with applying the Flux–Corrected–Transport procedure (Richtmyer & Morton 1967; Zalesak 1979). The predictor-corrector type of approximation was used. Equation (3) was replaced by its equivalent for the y -component of the vector potential to ensure the divergence-free property of the magnetic field. The equation of heat conduction was treated separately by the alternate direction implicit method with iterations. Transport coefficients for heat conduction and viscosity are taken from Braginski, 1965. In the code, the Bremsstrahlung radiation accounts for E_R

(Mahajan *et al.* 2001), using a somewhat modified formula assuming it to be 2 times greater, $E_R = 2 \cdot E_{Br} = 2 \cdot 1.69 \cdot 10^{-25} \cdot n^2 \cdot T^{1/2} \cdot Z^3 \text{ erg/cm}^3 \text{ s}$, ($Z = 1$). Since we were exploring a particular heating mechanism suggested there, no external heating source E_H was needed. A numerical mesh of 280×220 points was used for computation. The corresponding scheme is characterized by second order accuracy with respect to the chosen grid.

The latest observations support the idea that the coronal material is injected discontinuously (in pulses or bunches, for example) from lower altitudes into the regions of interest (e.g., spicules, jet-like structures). A realistic simulation, then, requires a study of the interaction of both temporally and spatially nonuniform initial flows with arcade-like magnetic field structures. These "close to the actual" cases represent more vividly the dynamics of the flow acceleration process. Below we study the dynamics of spatially-temporally localized flow (initially a Gaussian, Fig.-s 1,3) entering the region nested with varying scale arcade-like closed field line structures. For better visualization of the results we take the symmetric case. The flow is assumed to be initially weak ($|\mathbf{V}|_{0max} \ll C_{s0}$). The initial ambient magnetic field was modelled as a single 2D arcade with circular field lines in the x - z plane (Fig.2 for the vector potential/flux function). The arcade field attains its maximum value $B_{max}(x_0, z = 0) \equiv B_{0z}$ at x_0 at its center, and is a decreasing function of the height z (radial direction). This field was assumed to be initially uniform in time. When doing so, we choose the parameters to satisfy the observational constraint that, over a period of some tens of minutes, the location of the trapping/acceleration must have a relatively smooth evolution. The final shape and location of the structure of the associated $\mathbf{B}(\mathbf{r}, t)$, for example will be naturally defined by its material source, by the process dynamics, and by the initial field $\mathbf{B}_0(\mathbf{r}, t)$. We use the following representation for the magnetic field: $\mathbf{B} = \nabla A_y + B_z \hat{\mathbf{z}}$ and for given geometry $\mathbf{A}(0; A_y; 0)$; $\mathbf{b} = \mathbf{B}/B_{0z}$; $b_x(t, x, z \neq 0) \neq 0$. From numerous runs on the flow-field evolution, we have chosen to display pictorially the results corresponding to the following initial and boundary conditions: $B_{0z} = 100 \text{ G}$ and flow parameters: $V_{max}(x_0, z = 0) = V_{0z} = 2.18 \cdot 10^5 \text{ cm/s}$; $n_{0max} = 10^{12} \text{ cm}^{-3}$; $T(x, z = 0) = const = T_0 = 10 \text{ eV}$. The background plasma density $n_{bg} = 0.2n_{0max}$. In simulations $n(x, z, t = 0) = n/n_{0max}$ is an exponentially decreasing function of z . Experienced gained after numerous runs, revealing that the processes under study are localized within a small area of interaction, we settled on the following boundary condition, $\partial_x \mathcal{K}(x = \pm\infty, z, t) = 0$ which was used with sufficiently high accuracy for all parameters $\mathcal{K}(\mathbf{A}, T, \mathbf{V}, \mathbf{B}, n)$. Guided by observations we assume that the initial velocity field has a pulse-like distribution (Fig.3) with a time duration (life-time) $t_0 \gtrsim 50 \text{ s}$.

To illustrate the acceleration of initial flows (extremely weak), we have modelled several cases with different initial and boundary conditions. The dynamical picture is strongly de-

pendent on the relative strengths of the initial flow pressure and the magnetic field strength.

Our typical representative example is the evolution of a symmetric weak up–flow with its peak located in the central region of a single closed magnetic field structure (location of field maximum $B_{0z} = 100 G$) (Figs. 1-3). Figs. (4-8), in which we give the $x - z$ contour plots of all the relevant fields (A_y ; $|\mathbf{b}|$; n ; $|\mathbf{V}|$; T), contain the essence of the simulation. We find that the acceleration is significant in the vicinity of the field–maximum with strong deformation of field lines and energy re–distribution. In this very region, the simulations show cooling of the flow with serious density redistribution: part of the flow is trapped in the maximum field localization area, accumulated, cooled and accelerated. The accelerated flow reaches $\gtrsim 100 \text{ km/s}$ value in less than 100 s (in agreement with recent observations (Ryutova & Tarbell 2003; Seaton *et al.* 2001; Schrijver *et al.* 1999) and references therein). The accelerated flow is decoupled from the mother flow, and is localized in a distinguishable region with dimensions $\lesssim 0.05 R_s$ starting at a distance $\sim 0.01 R_s$ from the interaction surface. The time for reaching the quasi–equilibrium parameters is determined by the initial and boundary conditions (this conclusion is general for all cases).

In a stationary analysis to be presented in the next sub–section, we will attempt to derive the characteristic steady state parameters (like the distance from the surface) of the simulated system.

Extensive simulation experiments show that, when viscosity and heat flux effects are included, the flow acceleration evolution parameters depend strongly on α_0 , the parameter measuring the strength of the Hall term in the two–fluid equations. A very interesting and far-reaching result is that the final parameters of the accelerated flow are practically independent of the initial flow–characteristics (Fig.-s 4-8); only the initial fast stage of acceleration up to $\sim 200 \text{ km/s}$ is slightly different for different primary flows. Simulation results for 2 different initial life–times of the flow ($t_0 = 1000 \text{ s}$ – left panel and $t_0 = 100 \text{ s}$ – right panel in Fig.-s 4-8) illustrate this feature.

We also found that at some critical time, the solutions split into two parts; all fields, the magnetic (Fig.-s 4,5), the density (Fig.6), the velocity (Fig.7) and temperature (Fig.8) exhibit bifurcation. This process persists for different initial conditions. In Fig.9 we give time evolution plots of the maximum values of all fields (A_y , $|\mathbf{b}|$, b_p , b_z , n , $|\mathbf{V}|$, V_p , V_z , T) for a pulse–like flow interacting with a single arcade–structure for different initial life–times (t_0) of the flow ($t_0 = 100 \text{ s}$ (black); $t_0 = 1000 \text{ s}$ (red); $t_0 = 2000 \text{ s}$ (blue); $t_0 \rightarrow \infty$ (green)). In Fig.10 the same maximum values of all fields are plotted versus the initial life–time (t_0) of the flow for different time–frames ($t = 200 \text{ s}$ (black); 500 s (red); 1000 s (blue); 1500 s (green); 2000 s (lightgreen); 3000 s (rose)).

These pictures clearly demonstrate that the accelerated mother flow bifurcates into 2 separate fast daughter-flows (after an initial acceleration stage) modifying significantly the original arcade structure. The characteristic fields undergo rather similar dynamics for flow pulses with different initial life-times. It should be emphasized that now the maxima of these parameters are localized not along the initial B-maximum but on both sides of it and shifted along height (in the localization areas of each accelerated daughter flow with newly created B-maxima and currents). After the initial acceleration stage, the magnetic energy maxima remain practically unchanged up to some "blow-up" time ($\gtrsim 2000$ s) at which the gradients become too steep and the simulation results cease to be meaningful. The same result holds for the maxima of the transverse and parallel magnetic field energies (with $\lesssim 10\%$ accuracy). For fixed $T_0(\beta_0)$ the maximum values of each parameter (local in space) exhibit practically similar dynamics (independent of the initial flow life-time) reaching similar numbers at near-critical time. This picture persists for different initial $T_0(\beta_0)$. Testing the conservation of the total energy of the system as it evolves in time also shows that the simulation results can be trusted only up to the blow-up time; as one approaches this time the energy conservation no longer holds. To study longer time dynamics, the code will need improvement.

We will soon offer a possible explanation of these results through a simple equilibrium analysis.

We are now in a position to list the most interesting and distinguishable new results found in a 2.5D simulation of the two-fluid equations (containing various dissipative and short-scale effects) solved for different initial and boundary conditions:

1. A primary flow, even with a very slow initial speed ($V_{0z} \sim 1$ km/s locally sub-Alfvénic) is accelerated when it interacts with an arcade-like closed magnetic field structure. The effect is strong in the strong field region (initially the arcade center). This is a common feature independent of the arcade-characteristics, and the shape of the initial flow.
2. When viscosity and heat-flux are ignored, the time needed for the flow to acquire reasonable amount of energy is practically infinite. This is probably due to the fact that without dissipation, the energy transfer through the short-scales introduced by the two-fluid effects is not operative unless special conditions for catastrophic processes pertain.
3. For realistic α_0 (measuring the strength of the Hall term) the heat flux and viscosity effects cause a re-distribution of magnetic, flow kinetic and thermal energies in the arcade region in reasonable times ~ 100 s .

4. During the redistribution, the arcade field is modified; the thermal– and magnetic field– energies are converted to flow energy locally. The time–scale for generating a reasonably fast flow ($V_{0z} \gtrsim 100$ km/s) is dictated by α_0 . For a given initial $T_0(\beta_0)$, the larger the α_0 , the faster the flow generation. The density is non–uniformly redistributed within the arcade span.
5. At some specific ”critical time” $\lesssim 1000$ s the accelerated flow bifurcates into two separate fast flows. At this moment the arcade is also split in two, each with its share of the accumulated particles. Two fast spicule–like structures, carrying vorticity and current, are decoupled from the mother flow. Their densities are similar to the initial density of the mother–flow.
6. Initially the amplification of the flow depends on the flow β_0 , the ratio of the thermal and the magnetic field energy.
7. The distance from the interaction surface where the bifurcation occurs is $\sim 0.01 R_s$. It is interesting to mention that this height is lower than the heights of the base of a typical hot coronal structure ((Schrijver *et al.* 1999; Mahajan *et al.* 2001) and references therein) and it seems to be comparable to the latest observational findings (Brynildsen *et al.* 2004; Woo & Habbal & Feldman 2004). Initially the fast flow localizes in the center of the original arcade, starting from this distance. After the bifurcation several flows appear with distinguishable dimensions ($\lesssim 0.05 R_s$) practically on similar heights.
8. For fixed initial T_0 , the final speed of accelerated flow and the picture of the modified field structure are independent of the initial flow life–time. This result seems extremely important in connection with the observed flows in the lower atmosphere. At $t \gtrsim 1000$ s velocities reach ~ 500 km/s or even greater ($\lesssim 800$ km/s) values. Such result persists for different $T_0(\beta_0)$.

We note here that at any quasi–equilibrium stage of the acceleration process, the nascent intermittent flows will blend and interact with pre–existing varying scale closed field structures (recall the fine structure of the solar atmosphere); the “new” flows could be trapped by other structures with strong/weak magnetic fields participating in creating different dynamical scenarios: heating of the new structure (Mahajan *et al.* 2001) could result, or an escape channel could be created (Mahajan *et al.* 2003; Woo & Habbal & Feldman 2004). Instabilities, generation of waves could also be triggered.

3.2. Quasi–equilibrium pathway of flow acceleration due to magneto–fluid coupling — restrictions and analysis

Both the observational evidence and the results of dynamical simulation point out that a typical solar structure passes through a quasi–equilibrium stage (possibly even a series of quasi–equilibria) before it reaches the final explosive or distortion/deformation stage leading to particle escape. Let us try to understand the physics of these quasi–equilibrium structures in terms of equilibrium two–fluid equations. We analyze the simplest two–fluid equilibria with $T = \text{const} \rightarrow n^{-1}\nabla p \rightarrow T\nabla \ln n$ (generalization to a homentropic fluid: $p = \text{const} \cdot n^\gamma$ is straightforward and was performed in numerical work (Mahajan *et al.* 2002)). The dimensionless equations describing the model equilibrium can be written as:

$$\frac{1}{n}\nabla \times \mathbf{b} \times \mathbf{b} + \nabla \left(\frac{r_{A0}}{r} - \beta_0 \ln n - \frac{V^2}{2} \right) + \mathbf{V} \times (\nabla \times \mathbf{V}) = 0, \quad (6)$$

$$\nabla \times \left[\left(\mathbf{V} - \frac{\alpha_0}{n} \nabla \times \mathbf{b} \right) \times \mathbf{b} \right] = 0, \quad (7)$$

$$\nabla \cdot (n\mathbf{V}) = 0, \quad (8)$$

$$\nabla \cdot \mathbf{b} = 0, \quad (9)$$

where $\mathbf{b} = \mathbf{B}/B_0$ and the following normalizations were used: $n \rightarrow n_0$ – the density at some appropriate distance from the solar surface ($\geq 2000 \text{ km}$), $B \rightarrow B_0$ – the ambient field strength at the same distance, $|V| \rightarrow V_{A0}$ and the dimensionless parameters are defined with n_0, T_0, B_0 taken at the same distance. In the non–dissipative limit, the system allows the well–known double Beltrami solutions :

$$\mathbf{b} + \alpha_0 \nabla \times \mathbf{V} = d n \mathbf{V}, \quad \mathbf{b} = a n \left[\mathbf{V} - \frac{\alpha_0}{n} \nabla \times \mathbf{b} \right], \quad (10)$$

where a and d are the dimensionless constants related to ideal invariants: the magnetic $h_1 = \int (\mathbf{A} \cdot \mathbf{b}) d^3x$ and the generalized $h_2 = \int (\mathbf{A} + \mathbf{V}) \cdot \nabla \times (\mathbf{A} + \mathbf{V}) d^3x$ helicities (Mahajan & Yoshida 1998; Mahajan *et al.* 2001). Substituting (10) into (6)–(8) one obtains the Bernoulli Condition

$$\nabla \left(\frac{2\beta_0 r_{c0}}{r} - \beta_0 \ln n - \frac{V^2}{2} \right) = 0, \quad (11)$$

relating the density with the flow kinetic energy, and solar gravity.

Equations (6), (10),(11) represent a close system. They may be easily manipulated to yield an alternative form ($g(r) = r_{c0}/r$)

$$\frac{\alpha_0^2}{n} \nabla \times \nabla \times \mathbf{V} + \alpha_0 \nabla \times \left[\left(\frac{1}{a n} - d \right) n \mathbf{V} \right] + \left(1 - \frac{d}{a} \right) \mathbf{V} = 0, \quad (12)$$

$$\alpha_0^2 \nabla \times \left(\frac{1}{n} \nabla \times \mathbf{b} \right) + \alpha_0 \nabla \times \left[\left(\frac{1}{an} - d \right) \mathbf{b} \right] + \left(1 - \frac{d}{a} \right) \mathbf{b} = 0. \quad (13)$$

$$n = \exp \left(- \left[2g_0 - \frac{V_0^2}{2\beta_0} - 2g + \frac{V^2}{2\beta_0} \right] \right). \quad (14)$$

Equations (12), and (14) can be solved for the density and the velocity field \mathbf{V} and then \mathbf{b} could be determined from (10).

In the Solar atmosphere one observes quasi-equilibrium magnetic structures with both homogeneous (practically anywhere) and inhomogeneous (especially in the Chromosphere and TR) densities. By invoking appropriate variational principles, one can show that the generic double Beltrami class of equilibria are accessible in all cases of interest: constant density, constant temperature, or when the plasma obeys an equation of state. Maximum analytical headway, however, is possible for constant density. In that case the Bertrami–Bernoulli system consists of a set of linear equations and has two well-defined scales of variation. Non-constant density does not lead to a linear chain (see (12), and (14)), but allows phenomena peculiar to nonlinear systems. It is the latter class of systems that we will deal with now.

We will now calculate the amplification conditions for inhomogeneous density flows in the chromosphere. We restrict to a one-D variation (along the height Z) and choose the constants $a \sim d = 100$ so that $(a - d)/ad \sim 10^{-6}$. This choice insures that two homogeneous Beltrami scales will be vastly different. Detailed algebraic derivation of the approximate formulas used below can be found in Appendix 1.

The principal results of Appendix 1 are that if $n \gg (ad)^{-1}$ (density fall in the region of interest is not more than 3 orders of magnitude), then

1) the transverse components of magnetic field vary keeping $b_x^2 + b_y^2 = b_{0\perp}^2 = const$.

2) The density and the velocity fields are related approximately by $|V|^2 = 1/d^2 n^2$ so that the magnetic energy does not change much, $|\mathbf{b}|^2 = const$ to leading order.

3) The Bernoulli condition transforms to the defining equation for density:

$$\left(-2\beta_0 n^2 + \frac{1}{d^2} \right) \frac{\partial n}{\partial z} = n^3 g. \quad (15)$$

We notice that for the density to drop with height, it has to be larger than $n_{min} = (2\beta_0)^{1/2} d$. The existence of n_{min} also implies via $V^2 = 1/d^2 n^2$ that the maximum allowed velocity is

$$|V_{max}| = \frac{1}{d n_{min}} = (2\beta_0)^{1/2}. \quad (16)$$

As one approaches the singularity at $n = n_{min}$, the spatial variation of density (and in particular of the velocity) becomes very large. In such a region of the steep fall in density and rise in velocity, the time-independent dissipationless approach will not be valid. The Bernoulli equation (15), however, clearly reveals the origin of the very fast first stage of dynamical acceleration found in the simulations. From Eq.(15) we also see that the distance over which the catastrophe appears is determined by the strength of gravity, $g(z)$. Eventual amplification of the flow is determined by the local value of β_0 . These simple consequences of the Bernoulli equation explain one of the most important findings of the simulation: for a fixed initial temperature, the final characteristic parameters of the accelerated flow (quasi-equilibrium after the fast stage of acceleration) do not depend on its initial state. For these gross features of the system, the value of α_0 as long as it is finite, is also quite irrelevant, it just determines how fast the transverse components of magnetic and velocity fields oscillate. However when dissipation is present, α_0 through the mediation of short-scale physics, plays a crucial role in the acceleration/heating processes.

In connection with this result it is interesting to mention that according to latest observations on the quasi-equilibrium coronal loops, the so called quasi-periodic intensity oscillations are found to propagate upwards with speeds of the order of the (adiabatic/isothermal) coronal sound speed ((De Moortel & Parnell & Hood 2003) and the references therein).

For structures with ($n = const$), there are two distinct scenarios for eruptive events in the current framework : (1) when a "slowly" evolving structure finds itself in a state of no equilibrium and (2) when the process of creating a long-lived hot structure is prematurely aborted; the flow shrinks/distorts the structure that suddenly shines and/or releases energy or ejects particles. The latter mechanism requires a detailed time-dependent treatment. The semi-equilibrium, collisionless magnetofluid treatment pertains only to the former case (Ohsaki *et al.* 2001; Ohsaki *et al.* 2002). In the references cited, the conditions for catastrophic transformations of an original DB (double Beltrami state) were investigated. It was shown that when the total energy of the original state exceeds a critical value, the DB equilibrium suddenly relaxes to a single Beltrami state corresponding to the larger macroscopic scale; at the transition, much of the magnetic energy $|\mathbf{b}|^2$ of the original state is converted to heat/flow kinetic energy.

4. Summary of the results and Conclusions

We have developed a 2.5 Dimensional dynamical code for two-fluid equations. The two fluid equations contain the Hall term ($\alpha_0 \neq 0$), the ion vorticity, heatflux and viscosity

effects. We have used the code for a systematic study of particle acceleration and energy re-distribution phenomena associated with the interaction of a primary plasma flow with closed field-line magnetic structures. We also developed simple analytical arguments to explain and understand essential features of the simulation results. The simulation and analytical effort have led us to several far-reaching results for the understanding of the solar atmosphere. Even at the cost of some repetition, we list the most important ones :

(1) A primary plasma flow (locally sub-Alfvénic) is accelerated when it impinges on an emerging/ambient arcade-like closed magnetic field structure. The effect is strong in the strong field region. It is found that the final state of the flow is quite insensitive to the details of initial and boundary conditions; the latter simply dictate the time-scale at which significant flow-energy is generated.

(2) It is shown that there is a redistribution of magnetic, flow-kinetic and thermal energies in the arcade region so that the original arcade field is modified, and thermal and field energies are converted to flow energy. The time-scale of the fast ($\gtrsim 100$ km/s) flow generation is dictated by α_0 , the measure of the Hall term .

(3) It is found that at some specific time the accelerated flow bifurcates into 2 separate fast flows with an accompanying split of the arcade each containing its share of the accumulated particles.

(4) Initially the amplification of the flow depends on β_0 as proven by the 1D analysis; it is shown for the first time that the distance on which it happens is $\sim 0.01 R_s$ (independent of α_0) from the interaction surface. Later the fast flow localizes (with dimensions $\lesssim 0.05 R_s$) in the upper center of the original arcade.

(5) It is shown that for fixed initial T_0 the final speed ($\gtrsim 500$ km/s) of the accelerated flow, and the shape of the modified field structure are independent of the initial flow life-time. Many of these parameters can be approximately calculated by analysis.

We have shown possible pathways for both dynamical and steady generation of fast flows. The cold flows originating, for example, in the lower chromosphere acquire energy as they meet and interact with emerging/ ambient magnetic fluxes; the trapping of an ionized $\gtrsim 3$ eV plasma by network/ inter-network structures takes place at the same time. In the presence of dissipation, these flows are likely to play a fundamental role in the heating of the finely structured solar atmosphere. The explicit purpose of this paper, however, was to demonstrate the generation of flows in the lower atmosphere feeding on the ambient magnetic energy. The flows, in turn, provide a steady and assured source of matter and energy for the formation and primary heating of the corona as well as for the creation of the solar wind. The agreement of our preliminary results with the observation data lends credence and promise to attempts, based on the exploitation of sub-coronal flows, to tackle unresolved problems

like the coronal heating and origin of the solar wind. We believe that the chromospheric mass outflows, spicules, explosive events in chromosphere, micro- and nano-flares, large coronal flares, erupting prominences and CMEs may happen separately but can also be parts of a more global dynamic process of coronal specific regional formation.

ACKNOWLEDGEMENTS

Authors are extremely grateful to Prof. E. Parker for his valuable discussions and encouragement. Authors thank Dr. E. Marsch and Dr. K.I. Nikol'skaya for interesting and useful discussions. Authors express their deepest thanks to Dr. R. Miklaszewski for his leading suggestions when constructing the improved code. All the authors thank Abdus Salam International Centre for Theoretical Physics, Trieste, Italy. The work of SMM was supported by USDOE Contract No. DE-FG03-96ER-54366. The work of NLS, SVM and KIS was supported by ISTC Project G-633.

Appendix 1 — Equilibrium analysis of particle acceleration for non-uniform density case due to Magneto-fluid coupling

Let's rewrite DB equations (10) in following way:

$$\alpha_0 \nabla \times \mathbf{b} = -\frac{1}{a} \mathbf{b} + n \mathbf{V}, \quad \alpha_0 \nabla \times \mathbf{V} = -\mathbf{b} + d n \mathbf{V}, \quad (1)$$

Let's define a vector:

$$\mathbf{Q} = \begin{pmatrix} \mathbf{b} \\ \mathbf{V} \end{pmatrix}, \quad (2)$$

then (1) may be written as:

$$\alpha_0 \nabla \times \mathbf{Q} = M \mathbf{Q}, \quad (3)$$

where

$$M = \begin{pmatrix} -a^{-1}, & n \\ -1, & d n \end{pmatrix}. \quad (4)$$

M can be diagonalized by a similarity transformation:

$$S M S^{-1} = \begin{pmatrix} \lambda_+, & 0 \\ 0, & \lambda_- \end{pmatrix}, \quad (5)$$

where $[\lambda^2 - (d n - a^{-1})\lambda + n(1 - d a^{-1}) = 0]$ $\lambda_{\pm} = \frac{1}{2}[(d n - a^{-1}) \pm \sqrt{(d n - a^{-1})^2 - 4 n}]$ are standard roots. S is found to be (n is a slowly varying parameter, see the Bernoulli condition – V^2 and g are slowly varying):

$$S = \begin{pmatrix} 1, & -(\lambda_+ + a^{-1}) \\ 1, & -(\lambda_- + a^{-1}) \end{pmatrix}. \quad (6)$$

Then, if density fall is at a much slower rate than the slow scale of the Beltrami system (λ_-/α_0), rewriting (3) as:

$$\alpha_0 \nabla \times S \mathbf{Q} = (S M S^{-1}) S \mathbf{Q} = \begin{pmatrix} \lambda_+, & 0 \\ 0, & \lambda_- \end{pmatrix} S \mathbf{Q}, \quad (7)$$

one finds:

$$S \mathbf{Q} = \begin{pmatrix} \mathbf{Q}_+ \\ \mathbf{Q}_- \end{pmatrix} = \begin{pmatrix} \mathbf{b} - (\lambda_+ + a^{-1}) \mathbf{V} \\ \mathbf{b} - (\lambda_- + a^{-1}) \mathbf{V} \end{pmatrix} \quad (8)$$

each obeying its own independent (fully de-coupled) equation:

$$\nabla \times \mathbf{Q}_{\pm} = \frac{\lambda_{\pm}}{\alpha_0} \mathbf{Q}_{\pm}. \quad (9)$$

Let's find the amplification conditions for flows (say in the chromosphere, where $a \sim d = 100$ so that $(a - d)/ad \sim 10^{-6}$). Assuming (this is found to be a restriction) $n \gg (ad)^{-1}$ — density fall is not more than 3 orders of magnitude, then

$$\lambda_+ \sim dn, \quad \lambda_- \sim \frac{a-d}{ad}. \quad (10)$$

Notice, that for realistic solar atmosphere parameters (chromosphere, TR, corona) $\alpha_0 \sim 10^{-9} - 10^{-11}$ and the fast Beltrami scale $\lambda_+/\alpha_0 \sim 10^{11} - 10^{13}$ is very oscillatory and its amplitude must go to zero. This gives a relation between the velocity and the magnetic field;

$$\mathbf{Q}_+ = \mathbf{b} - (dn - a^{-1})\mathbf{V} \simeq \mathbf{b} - dn\mathbf{V} = 0, \quad (11)$$

and the approximate equation for the pertinent solution takes the form

$$\nabla \times \mathbf{Q}_- = \frac{a-d}{ad\alpha_0} \mathbf{Q}_- \quad \text{with} \quad \mathbf{Q}_- = \mathbf{b} - \frac{\mathbf{V}}{d} \simeq \mathbf{b}. \quad (12)$$

Let's consider a 1D problem (Z along height, $b_0 = 1$ when normalized). Eq.(12) leads to:

$$\frac{\partial}{\partial z} (b_x^2 + b_y^2) = 0 \quad \implies \quad b_x^2 + b_y^2 = b_{0\perp}^2. \quad (13)$$

Then, using eq.(11), one has: $V_x^2 + V_y^2 = b_{0\perp}^2/d^2 n^2$. From Continuity Equation and DB condition: $V_z = V_{0z}/n \sim b_{0z}/dn$. Thus,

$$V^2 = \frac{1}{d^2 n^2}. \quad (14)$$

Eq.(14) converts the Bernoulli condition ($T_0 = const$) to:

$$\left(-2\beta_0 n^2 + \frac{1}{d^2} \right) \frac{\partial n}{\partial z} = n^3 g. \quad (15)$$

Notice, that maximum allowed velocity for this mechanism is (compare with the condition (10) of (Mahajan *et al.* 2002)):

$$|V_{max}| = \frac{1}{dn_{min}} = (2\beta_0)^{1/2}. \quad (16)$$

Analysis gives similar results for varying temperature ($T = n^{-\mu}$, $0 < \mu < 1$).

REFERENCES

- Aschwanden, M.J., Poland A.I., and Rabin D.M. 2001a, *Ann. Rev. Astron. Astrophys.*, 39, 175.
- Aschwanden, M.J. 2001b, *ApJ*, 560, 1035.
- Braginski, S.I. "Transport processes in a plasma," in *Reviews of Plasma Physics*, edited by M. A. Leontovich. Consultants Bureau, New York, (1965), Vol.1, p.205.
- Brynildsen, N., Maltby, P., Kjeldseth-Moe, O. & Wilhelm, K. 2004, *ApJ*, 612, 1193.
- Chertok, I.M., Mogilevsky, E.I, Obridko, V. N., Shilova, N. S. and Hudson, H. S. 2002, *ApJ*, 567, 1225.
- Christopoulou, E.B., Georgakilas, A.A., and Koutchmy, S. 2001, *Solar Phys.*, 199, 61.
- De Moortel, I., Parnell, C.E. and Hood, A.W. 2003, *Solar Phys.* 215, 69.
- Falconer, D.A., Moore, R.L., Porter, J.G. and Hathaway, D.H. 2003, *ApJ*, 593, 549.
- Feldman, U., Landi, E. and Curdt, W. 2003, *ApJ*, 585, 1087.
- Goodman, M.L. 2001, *Space Sci. Rev.*, 95, 79.
- Goodman, M.L. 2000, *ApJ*, 533, 501.
- Hollweg, J.V., 1999, *J. Geophys. Res.*, 104, 505.
- Liu, Y., Jiang, Y., Ji, H., Zhang, H. and Wang, H. 2003, *ApJ*, 593, L137.
- Magara,T. and Longcope, D.W. 2003, *ApJ*, 586, 630.
- Mahajan, S.M., Miklaszewski, R., Nikol'skaya, K.I., and Shatashvili N.L., February 1999, Preprint IFSR #857, *The University of Texas, Austin*, 67 pages.
- Mahajan, S.M., Miklaszewski, R., Nikol'skaya, K.I., and Shatashvili, N.L. 2001, *Phys. Plasmas*, 8, 1340.
- Mahajan, S.M., Nikol'skaya, K.I., Shatashvili, N.L. & Yoshida, Y. 2002, *ApJ*, 576, L161.
- Mahajan, S.M., Miklaszewski, R., Nikol'skaya, K.I. and Shatashvili, N.L. 2003, ArXive: astro-ph/0308012.
- Mahajan, S.M., and Yoshida, Z. 1998, *Phys. Rev. Lett.*, 81, 4863.

- McKenzie, J.F., Sukhorukova, G.V. and Axword, W.I., 1998, *Astronomy and Astrophys.* 330, 1145.
- Nikol'skaya, K.I., and Valchuk, T.E. 1998, *Geomagnetizm and Aeronomy*, 38, No. 2, 14.
- Nitta, N.V., Cliver, E. W. and Tylka, A.J. 2003, *ApJ*, 586, L103.
- Ohsaki, S., Shatashvili, N.L., Yoshida, Z., and Mahajan, S.M. 2001, *ApJ*, 559, L61.
- Ohsaki, S., Shatashvili, N.L., Yoshida, Z., and Mahajan, S.M. 2002, *ApJ*, 570.
- Orlando, S., Peres, G., and Serio, S. 1995a, *Astrophys. and Astron.*, 294, 861.
- Orlando, S., Peres, G., and Serio, S. 1995b, *Astrophys. and Astron.*, 300, 549.
- Poedts, S., Rogava, A.D. and Mahajan, S. M. 1998, *ApJ*, 505, 369.
- Richtmyer, R.D. and Morton, K.W. *Difference Methods for Initial–Value Problems*. Interscience, New York, 1967.
- Ryutova, M. and Tarbell, T. 2003, *Phys. Rev. Lett.*, 90, 191101.
- Sakai, J.I., and Furusawa, K. 2002, *ApJ*, 564, 1048.
- Schrijver, C.J., Title, A.M., Berger, T.E., Fletcher, L., Hurlburt, N.E., Nightingale, R.W., Shine, R.A., Tarbell, T.D., Wolfson, J., Golub, L., Bookbinder, J.A., DeLuca, E.E., McMullen, R.A., Warren, H.P., Kankelborg, C.C., Handy B.N., and DePontieu, B. 1999, *Solar Phys.*, 187, 261.
- Seaton, D.B., Winebarger, A.R., DeLuca, E.E., Golub, L., and Reeves, K.K. 2001, *ApJ*, 563, L173.
- Socas–Navarro, H., and Sanchez Almeida, J. 2003, *ApJ*, 593, 581.
- Socas–Navarro, H., and Sanchez Almeida, J. 2002, *ApJ*, 565, 1323.
- Socas–Navarro, H., Martinez Pillet, V. and Lites, B.W. 2004, *ApJ*, 611, 1139.
- Socas–Navarro, H. 2004, *ApJ*, 613, 610.
- Socas–Navarro, H. and Lites, B.W. 2004, *ApJ*, 616, 587.
- Tu, C.-Y. and Marsch, E., 1997, *Solar Phys.*, 171, 363.
- Tu, C.-Y. and Marsch, E. 2001, *J. Geophys. Res.*, 106, 8233.

- Uchida Y., Miyagoshi, T., Yabiku T., Cable S., and Hirose S. 2001, *Publ. Astron. Soc. Japan*, 53, 331.
- Wilhelm, K. 2001, *Astrophys. and Astronomy*, 360, 351.
- Winebarger, A.M., DeLuca, E.E., and Golub, L. 2001, *ApJ*, 553, L81.
- Winebarger, A.R., Warren, H., Van Ballagooijen, A., DeLuca E.E., and Golub, L. 2002, *ApJ*, 567, L89.
- Woo, r, Habbal, S.R. & Feldman, U. 2004, *ApJ*, 612, 1171.
- Zalesak, S.T. 1979, *J. Comput. Phys.* 31, 335.
- Zhang, J., White, S.M. and Kundu, M.K. 1999, *ApJ*, 527, 977.
- Yang, G., Xu, Y., Cao, W., Wang, H., Denker, C. and Rimmele, T.R. 2004, *ApJ*, 617, L151.
- Yoshida, Z., Ohsaki, S. and Mahajan, S.M. 2004, *Phys. Plasmas*, 11, 3660.

Fig. 1.— Initial symmetric profiles of the radial velocity V_z , and density n . The respective maxima (at $x=0$) are $\sim 2 \text{ km/s}$ and 10^{12} cm^{-3} .

Fig. 2.— Contour plots for the y - component of vector potential A (flux function) in the $x - z$ plane for a typical ambient arcade-like solar magnetic field (initial distribution). The field has a maximum $B_{max}(x_0 = 0, z_0 = 0) = 100 \text{ G}$.

Fig. 3.— The original pulse is limited in time. A time plot of $V_{z,max}(t, z = 0)$ corresponding to the shape $V_z(t, z = 0) = V_{0z} \sin(\pi t/t_0)$; $V_z(t > t_0) = 0$. The parameter t_0 (1000 s for this pulse) can be interpreted as the "life-time" of the pulse.

Fig. 4.— $x - z$ contour plots at various time-frames: $t = 200 \text{ s}$; 500 s ; 1000 s ; 1500 s ; 2000 s ; 3000 s for the dynamical evolution of A_y for flows with two different initial life-times. The spatially and temporally inhomogeneous (type displayed in Fig.1, Fig.3) primary flows are accelerated as they make their way through the magnetic field with an arcade-like structure (Fig.2). The realistic viscosity and heat-flux effects as well as the Hall term ($\alpha_0 = 3.3 \cdot 10^{-10}$ realistic) are included in the simulation. Left panel corresponds to the case of initial flow life-time: $t_0 = 1000 \text{ s}$, right panel — for $t_0 = 100 \text{ s}$. There is a critical time ($\lesssim 1000 \text{ s}$) when the accelerated flow bifurcates in 2; the original arcade field is deformed correspondingly.

Fig. 5.— $x - z$ contour plots for the dynamical evolution of $|\mathbf{b}|$ exactly following the pattern of Fig.4. After the bifurcation (read caption of Fig.4), strong magnetic field localization areas, carrying currents, are created symmetrically about $x = 0$.

Fig. 6.— $x - z$ contour plots for dynamical evolution of density n exactly following the pattern of Fig.4. Post-bifurcation daughter flows are localized in the newly created magnetic field localization areas. The maximum density of each daughter flow is of the order of the density of the mother-flow. Daughter-flows have distinguishable dimensions $\sim 0.05 R_s$

Fig. 7.— $x - z$ contour plots for the dynamical evolution of $|\mathbf{V}|$ exactly following the pattern of Fig.4. The initial flow, locally sub-Alfvénic, is accelerated reaching significant speeds ($\gtrsim 100 \text{ km/s}$) in a very short time ($\gtrsim 100 \text{ s}$). The effect is strong in the strong field region (center of the arcade). At $t \gtrsim 1000 \text{ s}$, the velocities reach $\sim 500 \text{ km/s}$ or even greater ($\lesssim 800 \text{ km/s}$) values. The distance from surface where it happens is $\gtrsim 0.01 R_s$.

Fig. 8.— $x - z$ contour plots for dynamical evolution of temperature T exactly following the pattern of Fig.4. In the regions of localization of the daughter flow there is a significant cooling while the nearby regions are heated.

Fig. 9.— Dynamical evolution of the characteristic fields (their maximum values), $|\mathbf{b}|$; b_x ; b_y ;

n ; $|\mathbf{V}|$; V_x ; V_y ; T , defining the interacting flow–magnetic field system (their $x - z$ contour plots are shown in Fig.-s 4–8) for different initial flow life-times ($t_0 = 100\text{ s}$ (black); 1000 s (red); 2000 s (blue); ∞ (green)). The code ceases to be dependable for times at which very steep gradients emerge; the blow-up time for this simulation is ($\lesssim 3000\text{ s}$)

Fig. 10.— Maximum values of $|\mathbf{b}|$; b_x ; b_y ; n ; $|\mathbf{V}|$; V_x ; V_y ; T (their $x - z$ contour plots are shown in Figs. 4–8) versus the initial life-time (t_0) of the primary outflow for different time-frames ($t = 200\text{ s}$ (black); 500 s (red); 1000 s (blue); 1500 s (green); 2000 s (lightgreen); 3000 s (rose)). The code ceases to be dependable for times at which very steep gradients emerge; the blow-up time for this simulation is ($\lesssim 3000\text{ s}$)

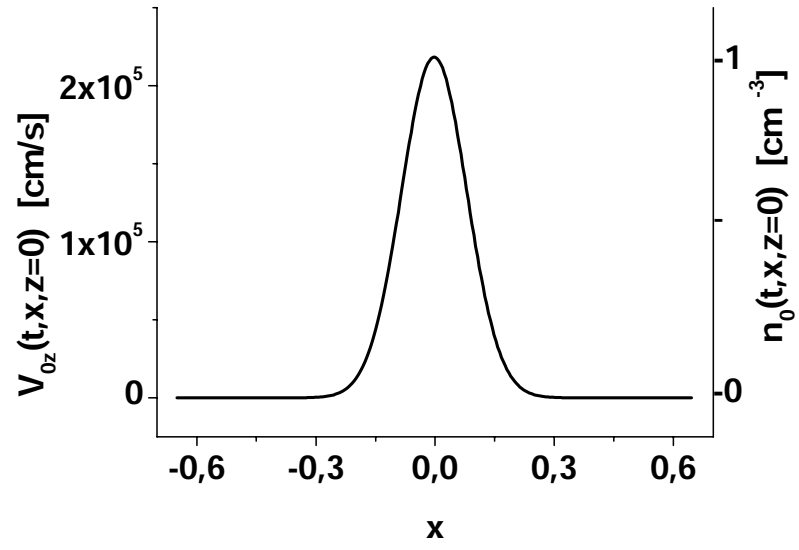


Fig.1

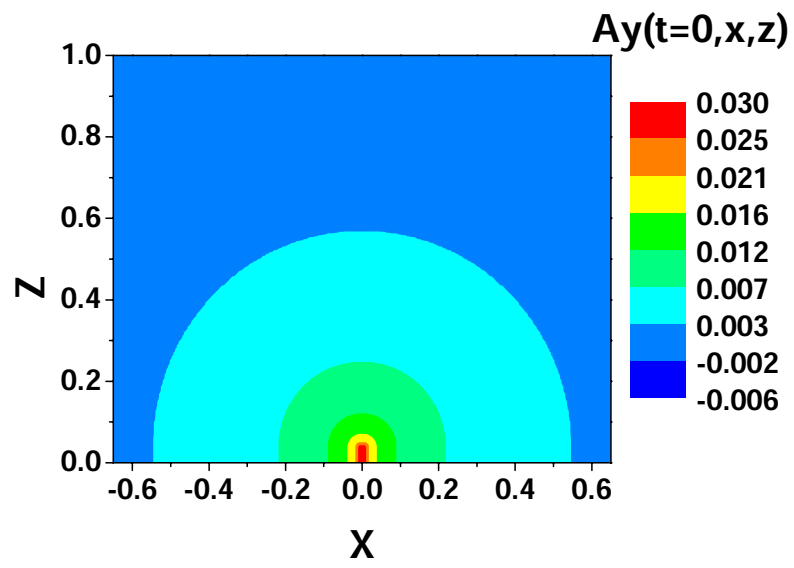


Fig.2

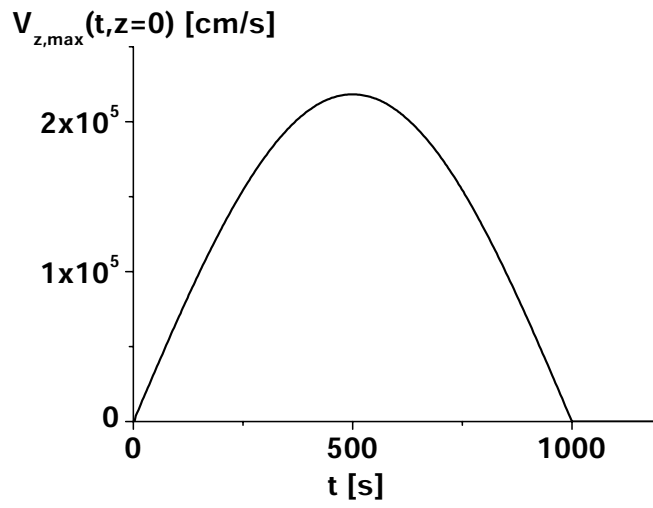
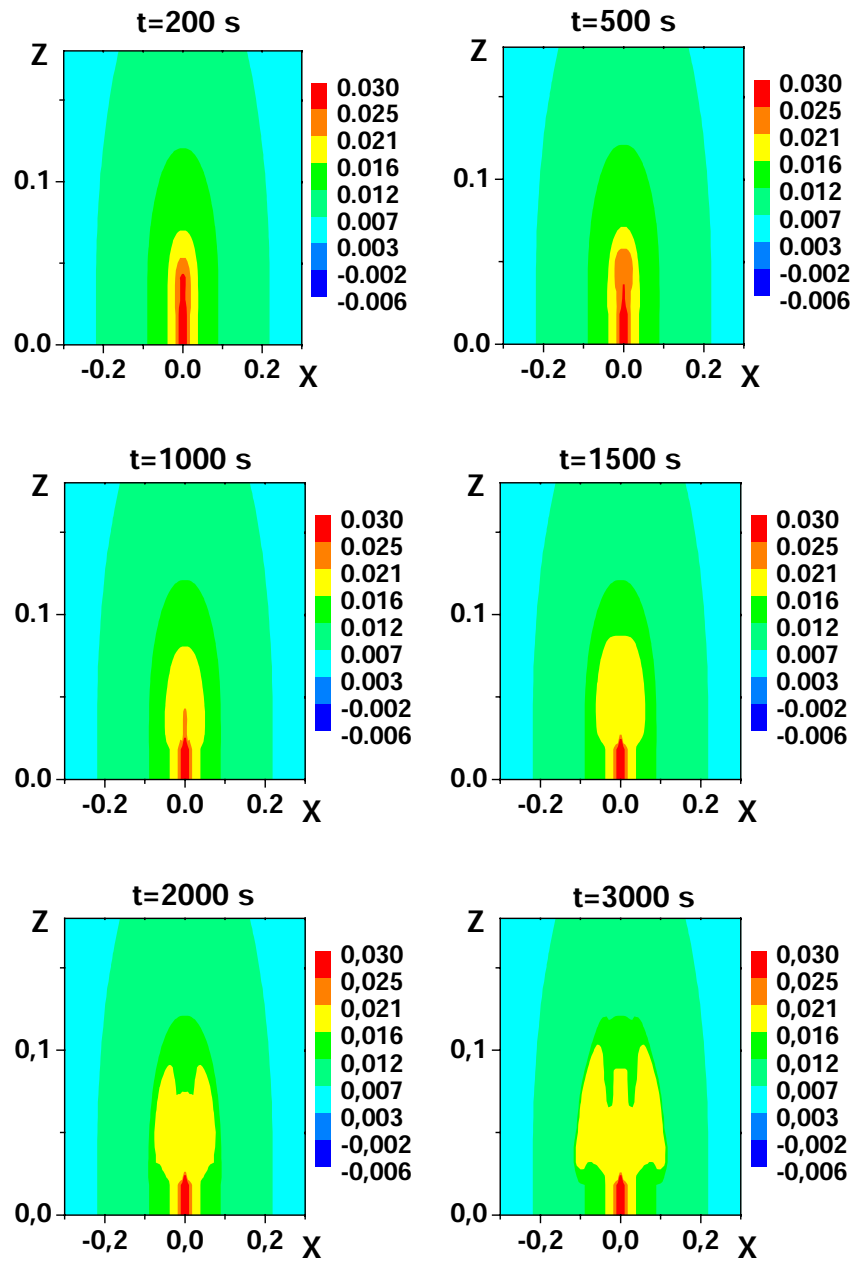


Fig.3

$t_0=1000s$



A_y

$t_0=100s$

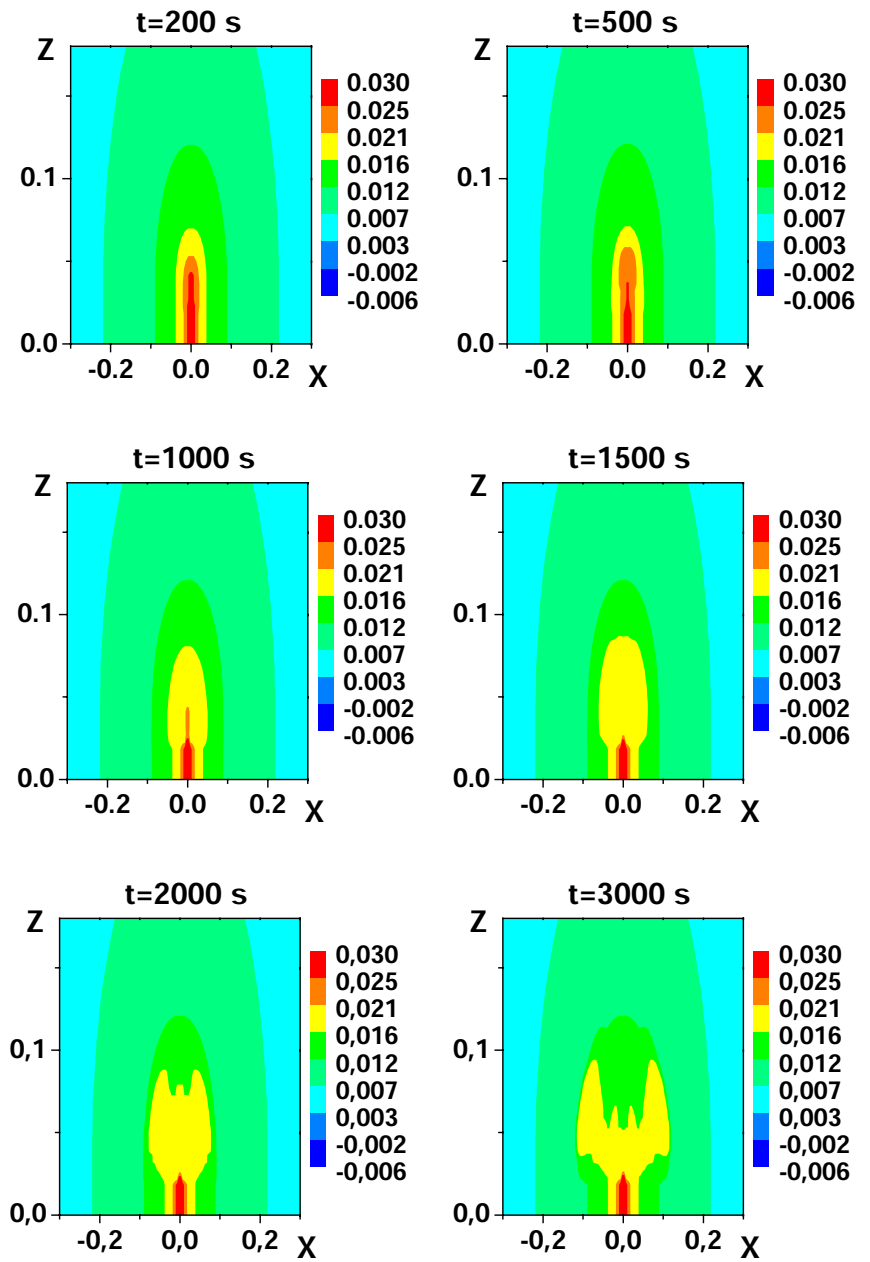
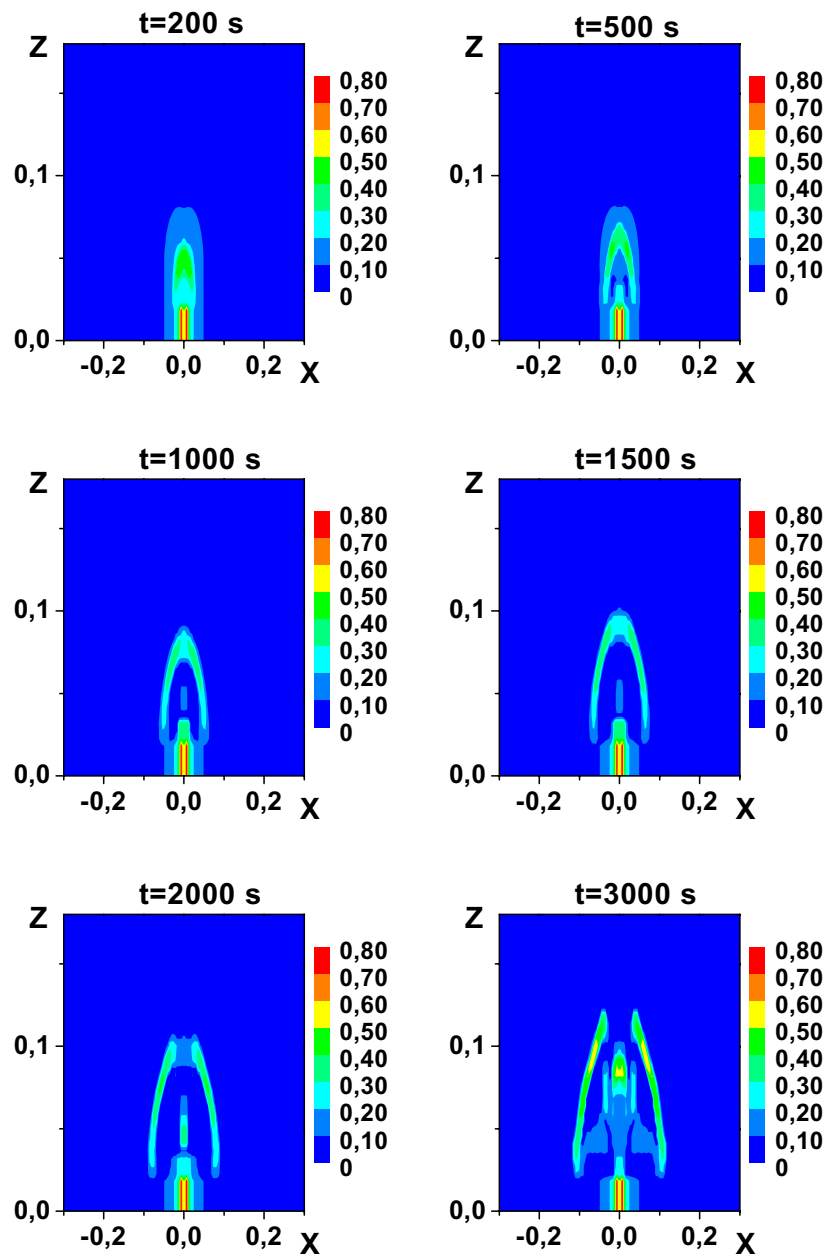


Fig.4

$t_0=1000s$



|b|

$t_0=100s$

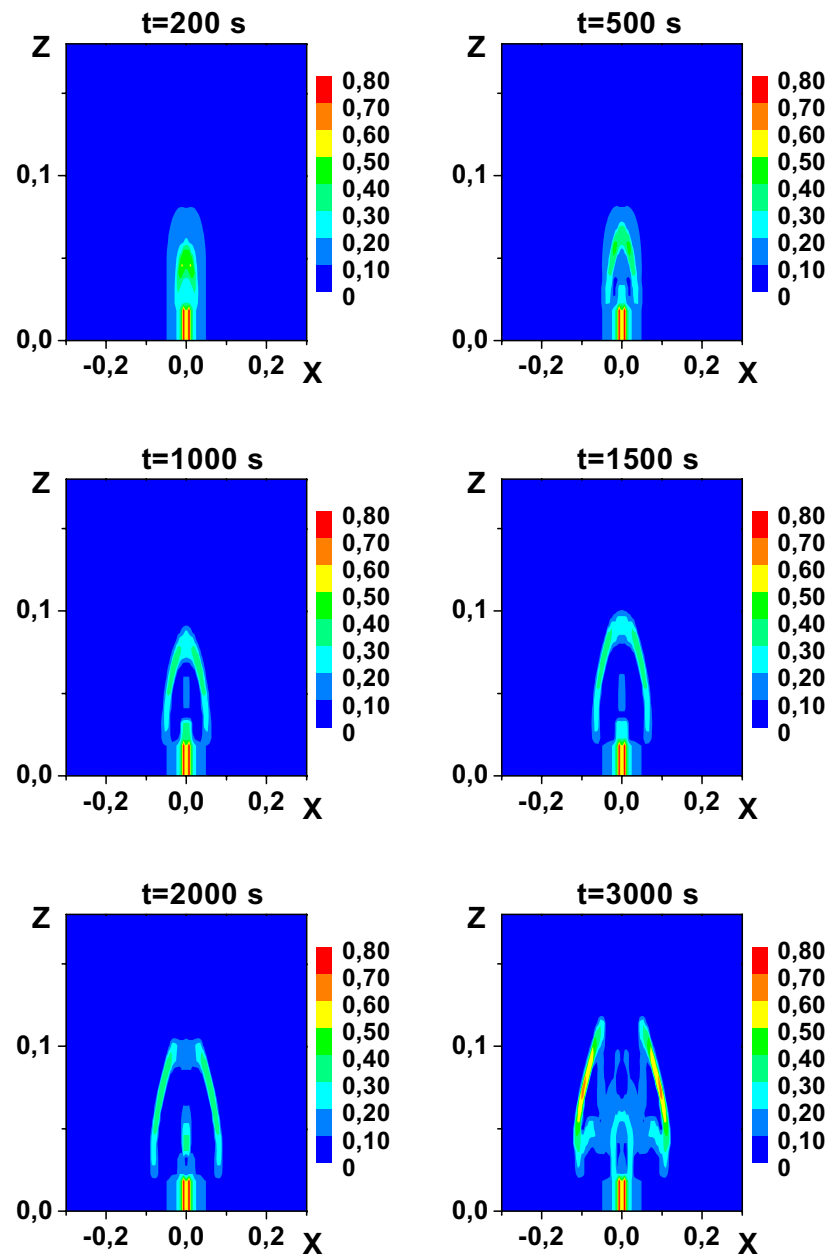


Fig.5

$t_0 = 1000s$

n

$t_0 = 100s$

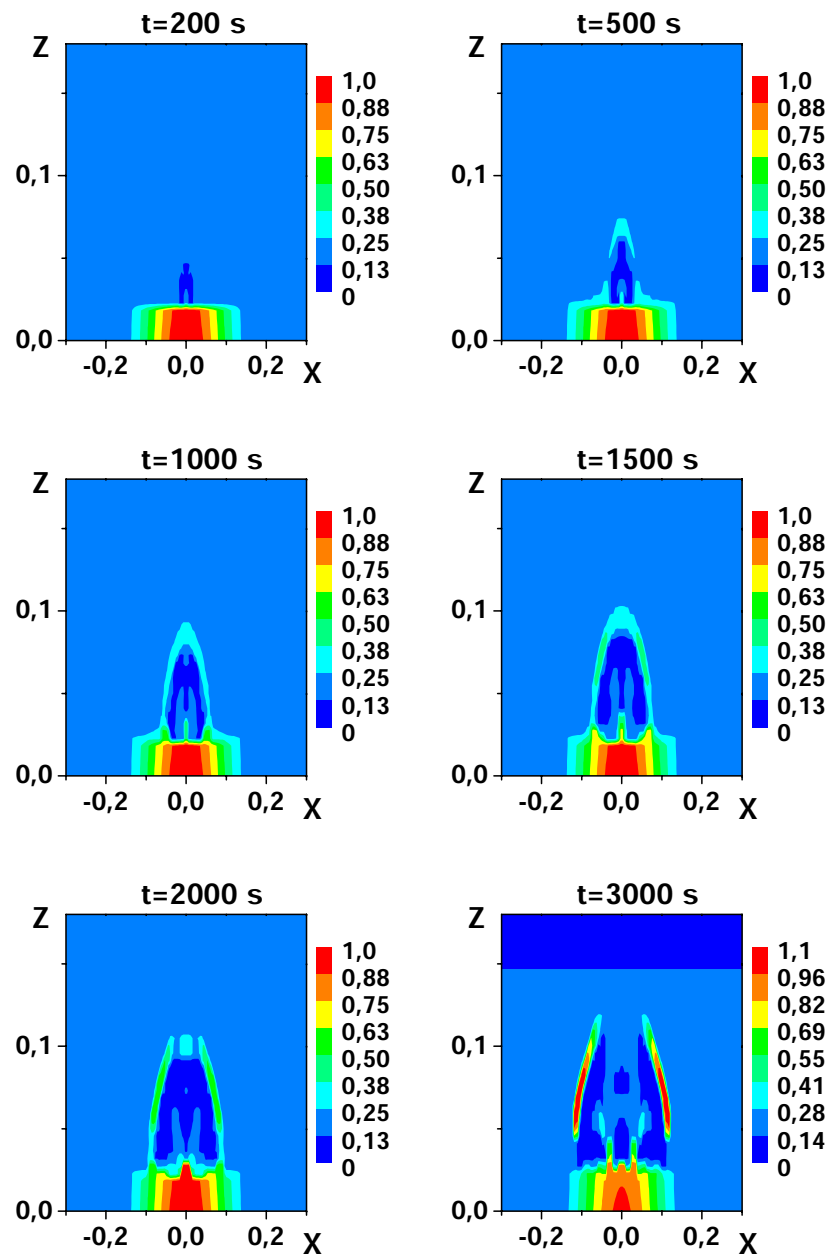
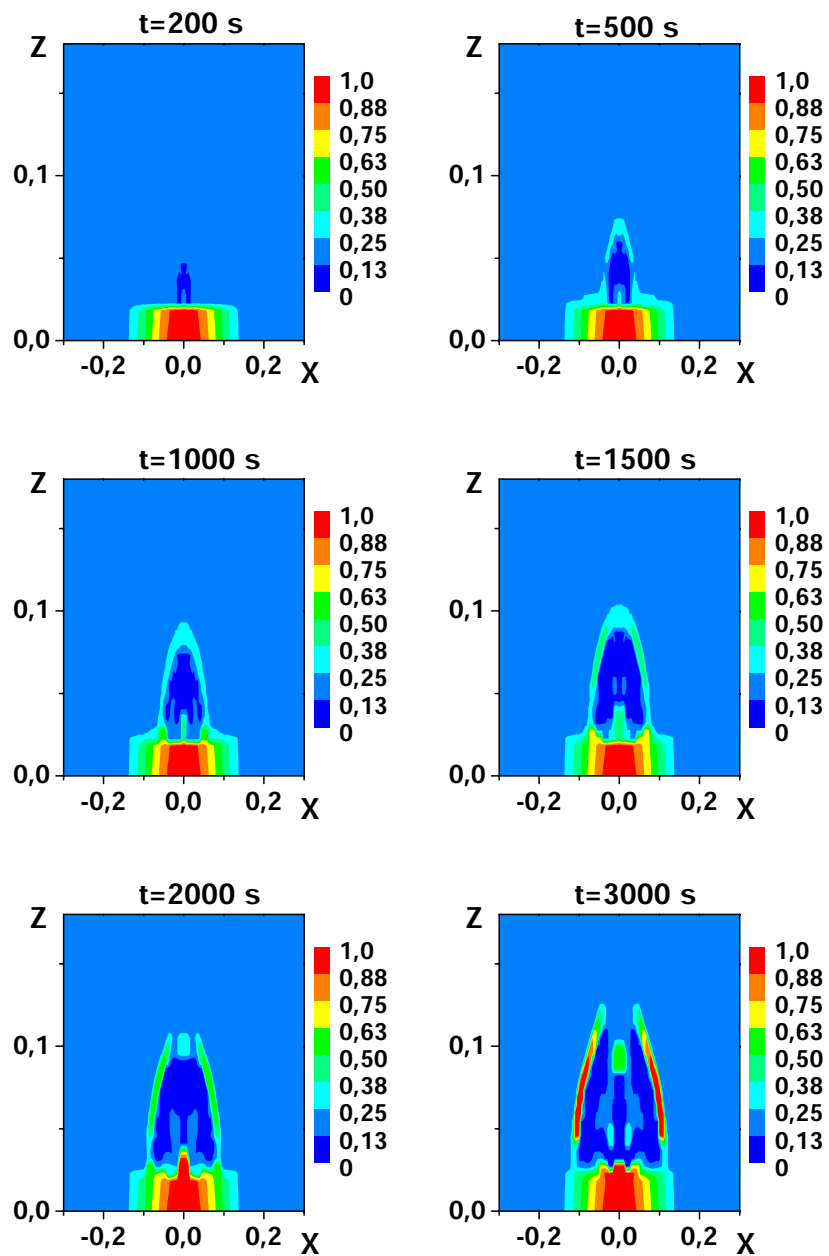


Fig.6

$t_0 = 1000s$

$|V|$

$t_0 = 100s$

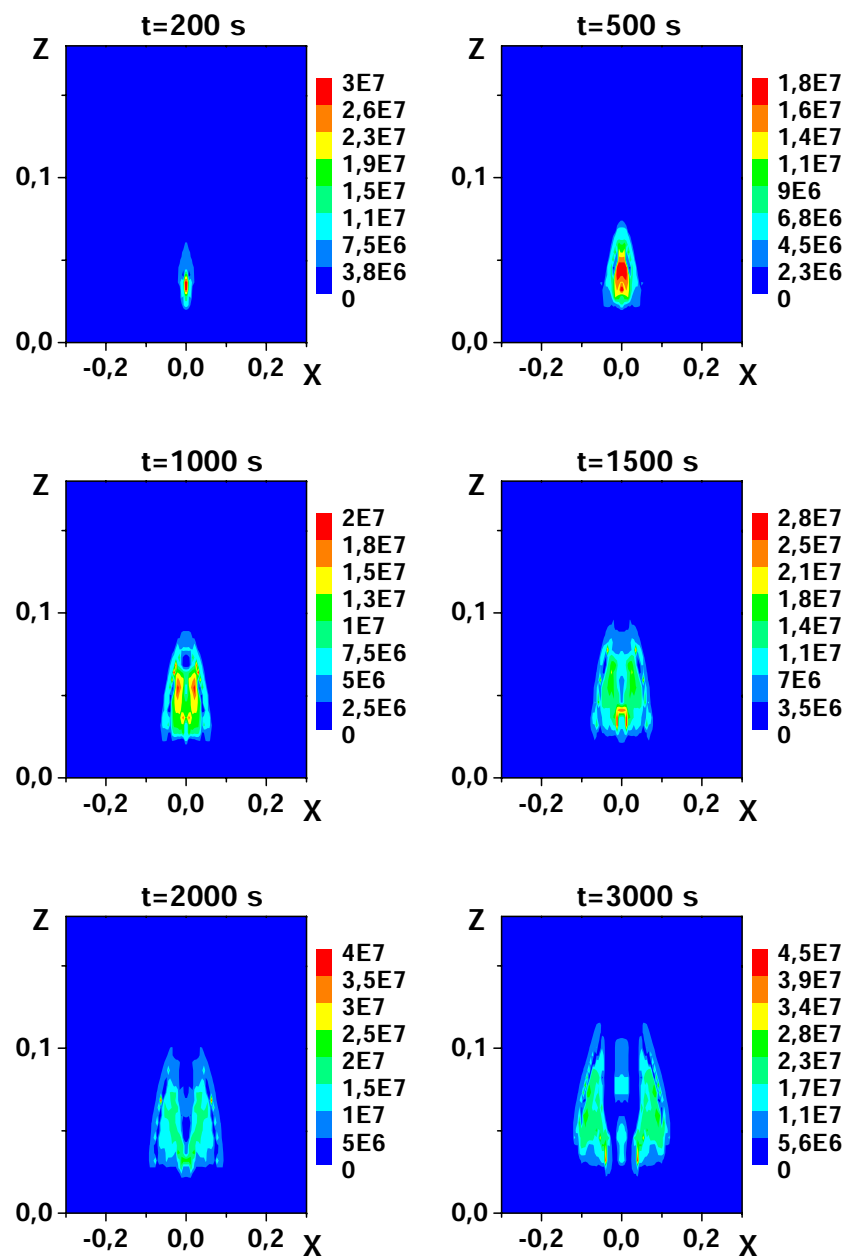
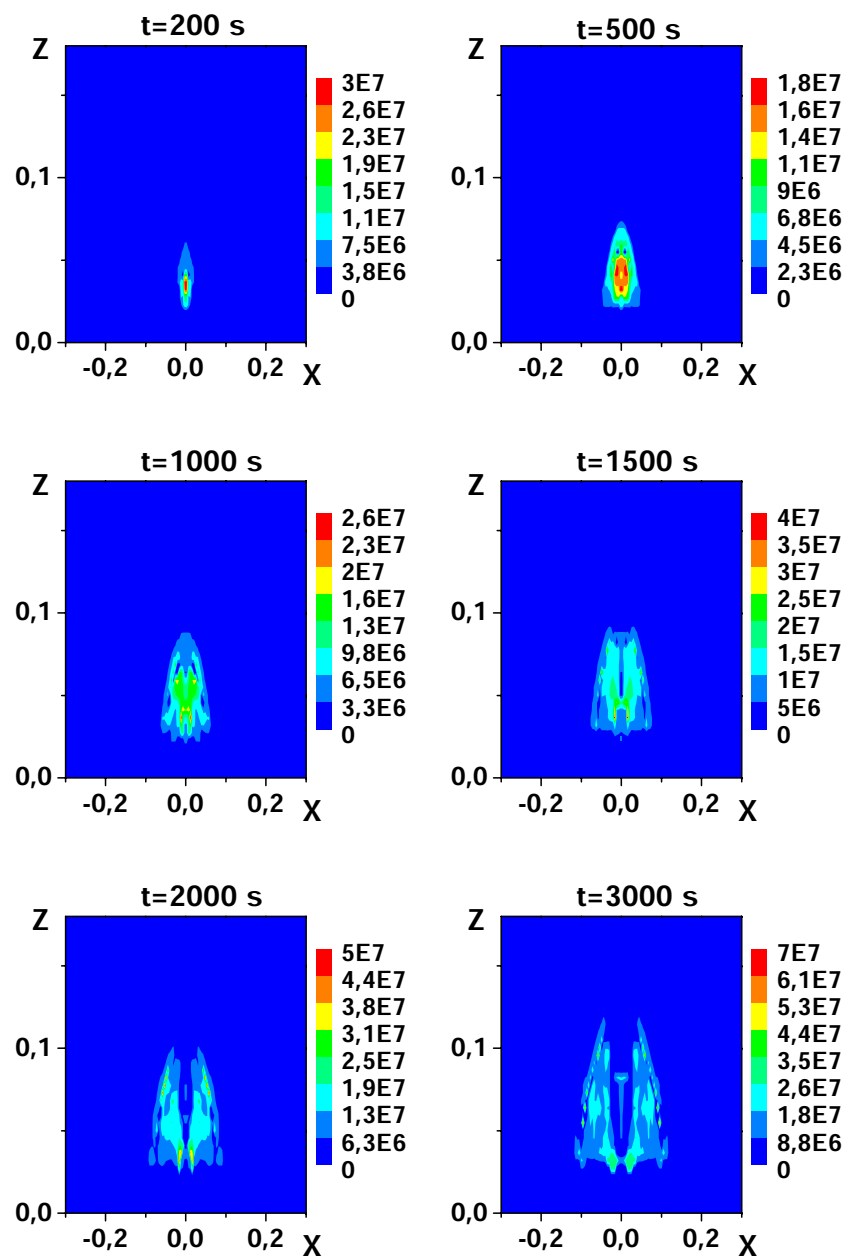


Fig.7

$t_0 = 1000s$

T

$t_0 = 100s$

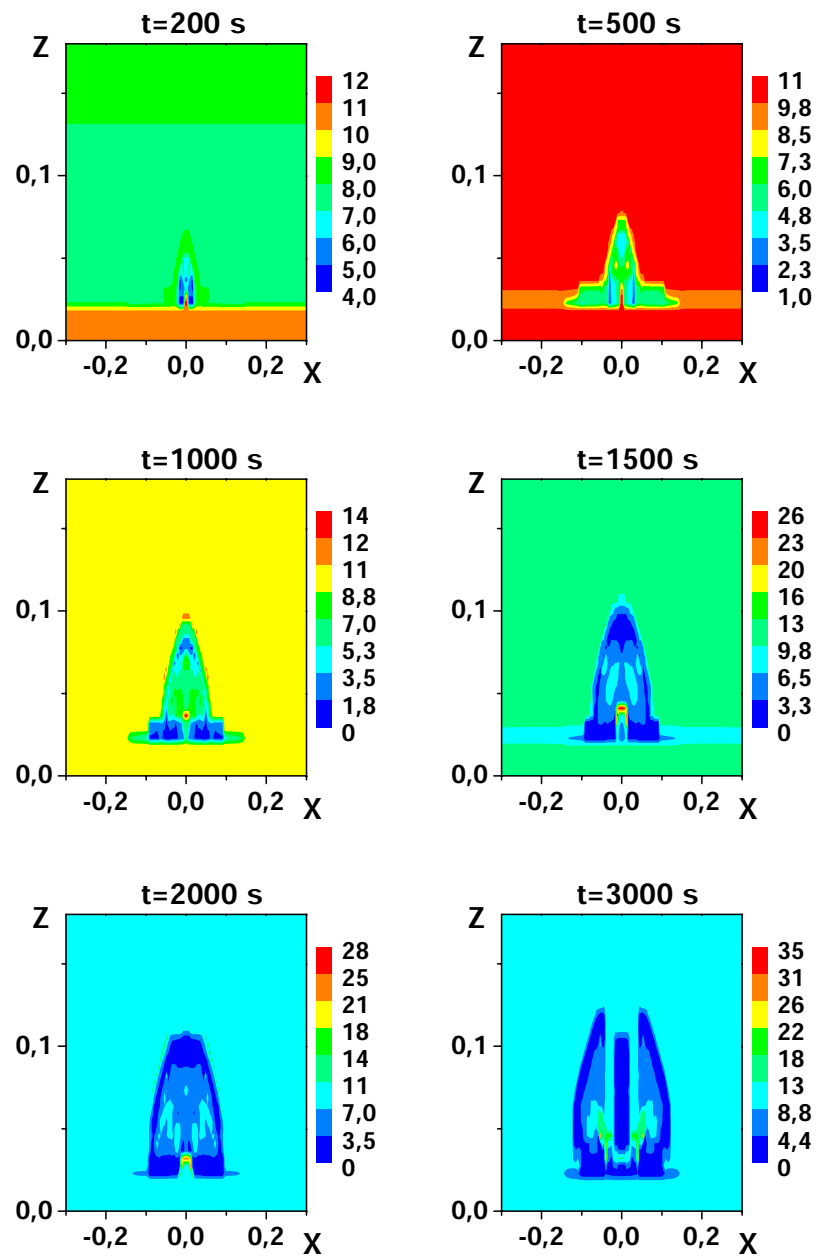
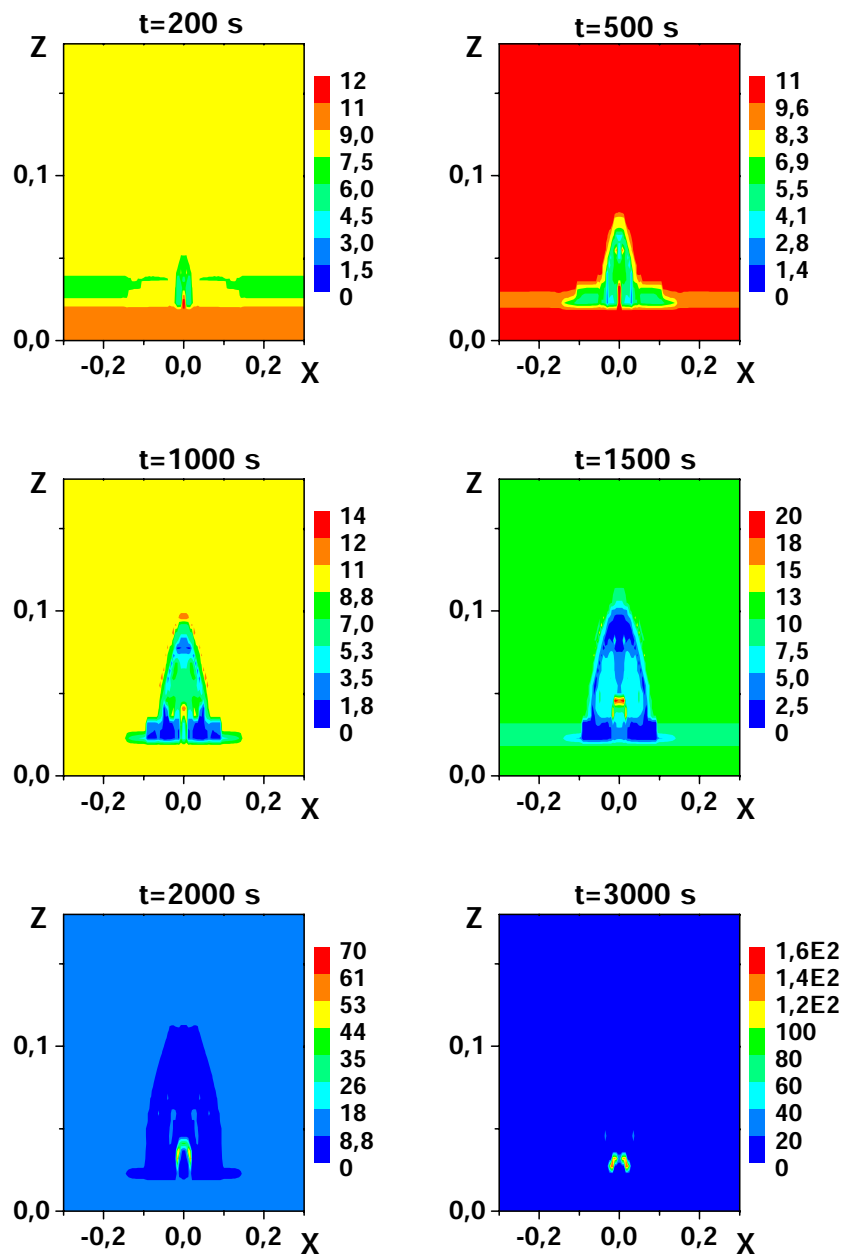


Fig.8

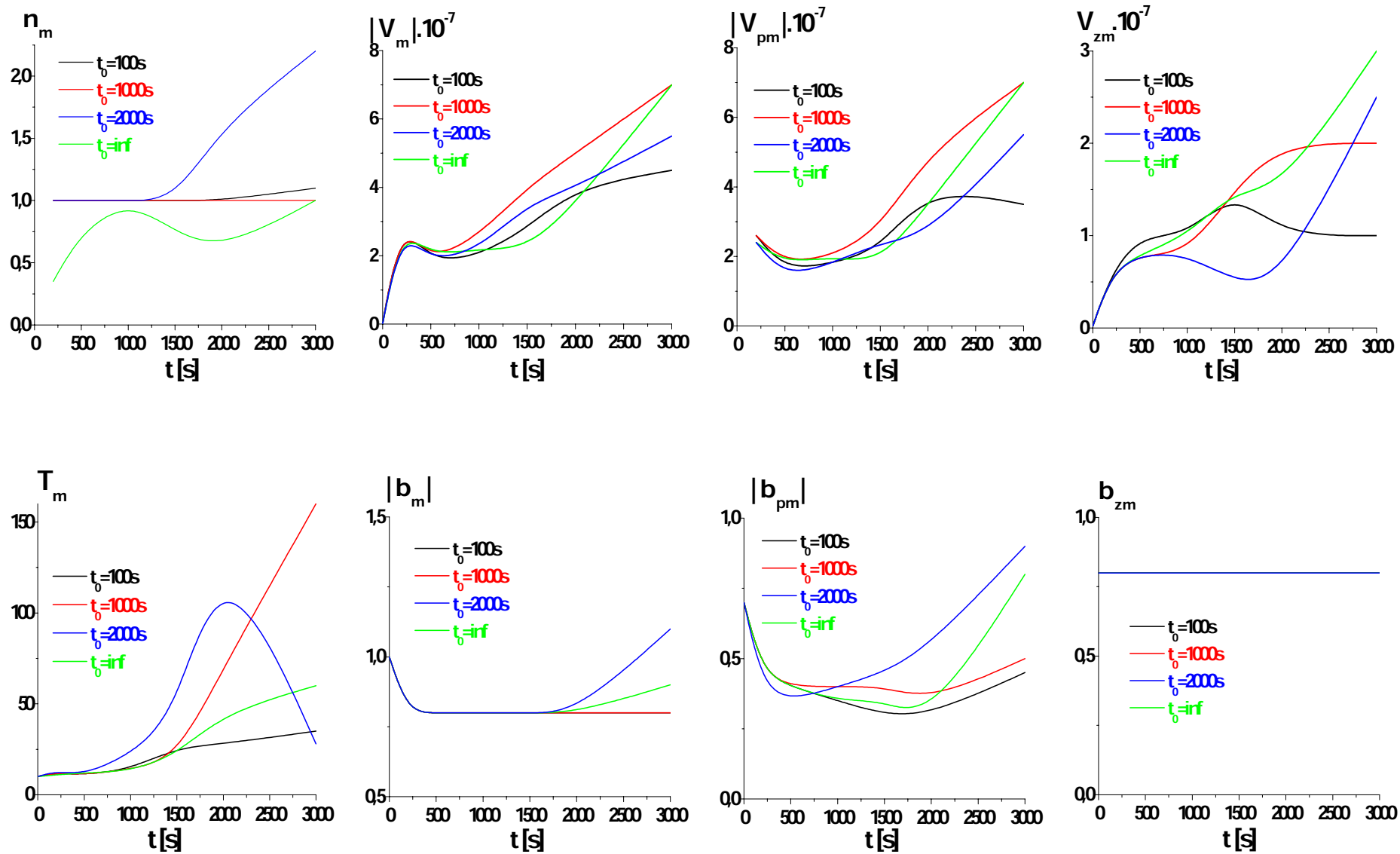


Fig.9

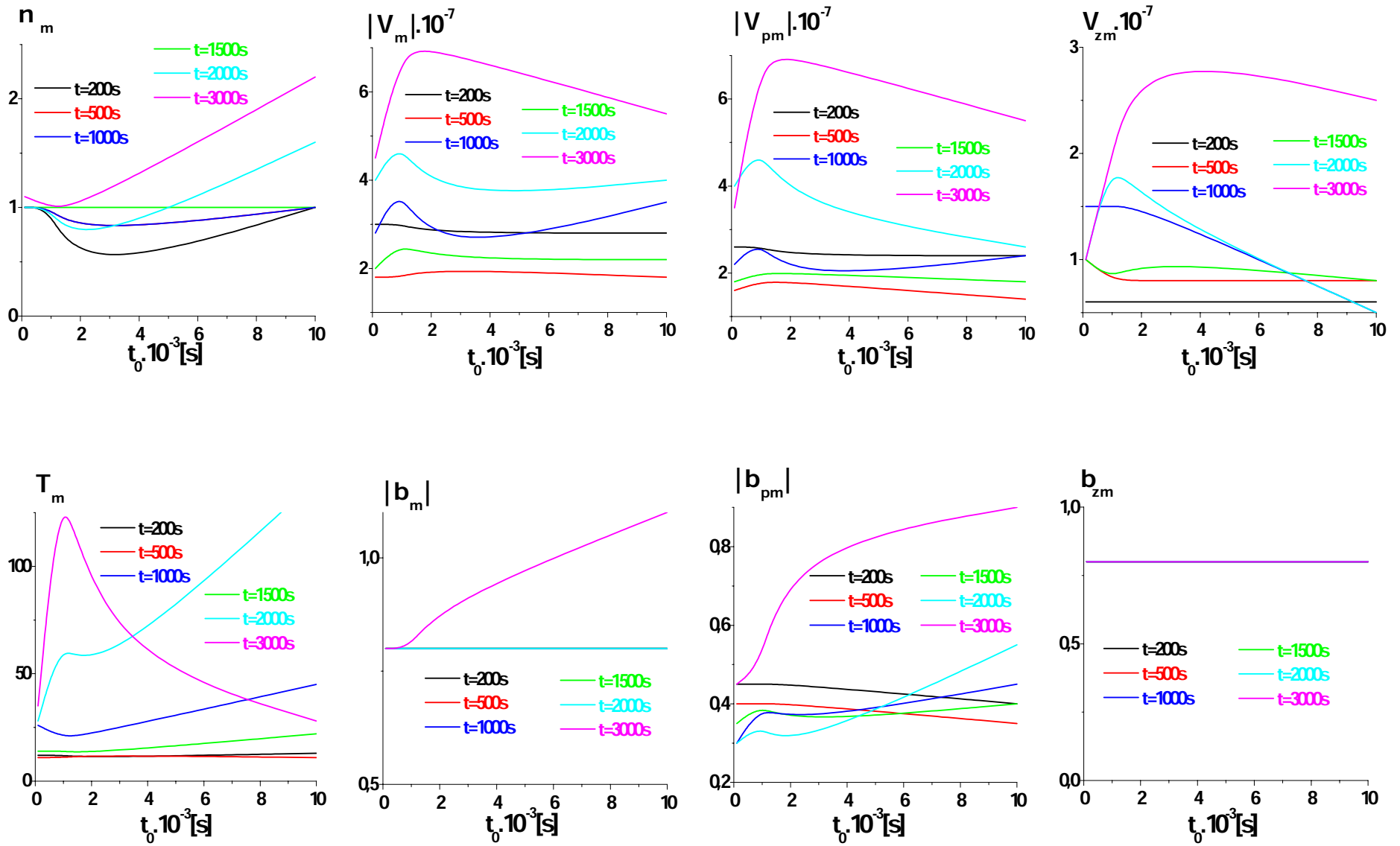


Fig.10